Aspherical and covalent bonding character of *d* electrons of molybdenum from synchrotron x-ray diffraction

Journal of Physics Communications

OPEN ACCESS

RECEIVED
19 June 2019

REVISED
24 August 2019

ACCEPTED FOR PUBLICATION
5 September 2019

PUBLISHED
16 September 2019

PAPER

Aspherical and covalent bonding character of *d* electrons of molybdenum from synchrotron x-ray diffraction

Tomoaki Sasaki[1], **Hidetaka Kasai**[1,2,3] **and Eiji Nishibori**[1,2,3]

[1] Graduate School of Pure and Applied Sciences, University of Tsukuba, 305-8571, Japan
[2] Faculty of Pure and Applied Sciences, University of Tsukuba, 305-8571, Japan
[3] Tsukuba Research Center for Energy Materials Science, University of Tsukuba, 305-8571, Japan

E-mail: nishibori.eiji.ga@u.tsukuba.ac.jp

Keywords: x-ray charge density, synchrotron radiation, *d*-orbital

Abstract

The occupancies and spatial distribution of electrons for 4*d*-orbitals in pure molybdenum have been experimentally determined by a charge density study from synchrotron radiation x-ray powder diffraction. There are valence charge density maxima in interatomic positions indicating bond formation. The electron deficiencies of Γ_{12} orbitals were visualized in the observed static deformation density. An electron deficiency of ~0.5 was observed from the orbital population analysis through multipole refinement. The occupancies and spatial distribution have also been calculated by a density functional theoretical calculation using WIEN2k packages for comparison. The observed features agree well with the theoretical study. In addition, the observed charge density has more covalent bonding character than the theoretical one. The present study confirms that a state-of-the-art x-ray charge density study can reveal the spatial structure of *d*-electrons in 4*d*-system.

1. Introduction

Electrons in the *d*-orbitals of transition metals and their complexes govern their properties and functions. The magnetism of a simple transition metal is caused by the interaction between its *d*-electrons. Exotic properties such as superconductivity, multiferroicity, and colossal magnetoresistance were found in transition metal oxides. The properties are closely related to their electronic structure of the *d*-electron. The *d*-electrons have both an itinerant and localized character in the system. Characterization of the *d*-electron in the system is one of the main topics for condensed matter physics and considerable amounts of studies have been carried out to investigate the *d*-electron during the past one hundred years [1]. In particular, considerable research has been carried out for 3*d*-transition metal oxides during the last three decades after the discovery of the high-Tc superconductivity of copper oxide [2]. The heavier 4*d*- and 5*d*-elements and their complexes had been ignored until the discovery of the exotic superconductivity of Sr_2RuO_4 [3].

The spatial and energetic structures of *d*-electrons have been largely investigated both experimentally and theoretically. The distribution of *d*-electrons in 3*d*-transition metals [4–9] and their complexes [10, 11] have been observed by experimental charge density studies. Spectroscopic studies of 3*d*-transition metals [12–14] and their complexes [1, 15, 16] have also been carried out using optical [12, 14, 15, 17], photoemission, [1, 13, 16, 18] and x-ray absorption spectroscopies [19], among others. The spatial and energetic structures of the 3*d*-electrons have been revealed by the measurements. The energetic structure of the 4*d*- and 5*d*-system has also been investigated by the spectroscopies [20]. However, the spatial structure of the 4*d*- and 5*d*-system has never been revealed experimentally except for one example [8], as the contribution of the 4*d*- and 5*d*-electrons to x-ray diffraction is much lower than that of the 3*d*-system.

We have conducted accurate structure factor measurements for the charge density study from high energy x-ray diffraction (HXRD) of one of the largest third generation synchrotron radiation (SR) facility SPring-8. The highest precision of structure factor using the technique exceeds 0.1%, which is comparable to the extremely accurate Pendellosung fringe method [21] and quantitative convergent beam electron diffraction [22]. The

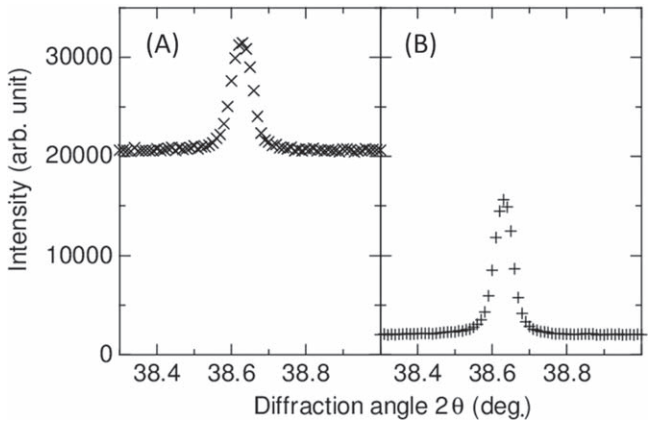

Figure 1. Plots of 620 reflection (A) for normal measurement and (B) using copper and nickel foils. The foils reduce fluorescence and characteristic x-ray intensities from molybdenum.

spatial distribution of small amounts of electrons such as the interlayer bonding electron of TiS_2 [23] and the conductive π-like electron of LaB_6 [24] have been revealed experimentally by SR-HXRD. It is essential to verify a performance of SR-HXRD for the visualization of 4*d*- and 5*d*-electrons. Typical materials with 4*d*- and/or 5*d*-electrons are required for this purpose.

Molybdenum is one of the simplest 4*d*-system. The electron configuration of molybdenum is $4d^5 5s^1$. The electronic structure of molybdenum was investigated by both theoretical and experimental studies [25–28]. The Fermi surface was investigated using de Haas-van Alphen measurements by several research groups [27, 28]. The band structure was determined by theoretical calculations [25, 26]. The experimental Fermi surface was consistent with that calculated from theory. Zunger *et al* [25] demonstrated that the *d*-electrons in the molybdenum comprise bonding orbital $d_{xy+yz+xz}$ and antibonding orbitals d_{z2} and d_{x2y2}. The electronic structure of molybdenum was investigated by the liner combination of Gaussian orbitals method (LCGO) [26]. The density of states, Fermi surface, charge form factors, Compton profiles, and optical conductivity were theoretically estimated by this method. The electron density distribution in real space from the experimental results will provide a further understanding of molybdenum. In this study, we completed a charge density study of molybdenum using the SR-HXRD technique [29].

2. Experiment and analysis

Molybdenum powder with 99.9% purity and 3–5 μm average particle size was used as a sample. The powder was sealed in a 0.2 mmϕ Lindemann glass capillary with argon gas. Synchrotron powder x-ray diffraction data were measured at SPring-8 BL02B2. Imaging Plate (IP) was used as a detector. The wavelength of the incident x-ray was 37.7 keV calibrated by the lattice constant of the National Institute of Standards and Technology (NIST) CeO_2 standard sample. The temperature of the sample was controlled at 30 K using a He gas flow low-temperature device. Two two-dimensional powder images were measured. One of which was measured by moving detector position to a high scattering angle region in 2θ to improve the counting statistics and to extend the reciprocal resolution.

The size of the perfect crystal region for molybdenum is estimated less than 1 μm from peak width of powder profiles. In the case of 1 μm, the largest extinction factor is 0.2% at $hkl = 110$, where the extinction factor is approximated by $y \approx \exp[-(l/2l_L)]$, l is the size of the perfect crystal region, and l_L is the extinction length [30]. It is estimated by $l_L = (\pi v_c \cos\theta_B)/(2|P| r_e \lambda |F|)$, where v_c is the volume of unit cell, θ_B is Bragg angle, $|P|$ is polarization factor, r_e is classical electron radius, and $|F|$ is absolute value of structure factor. In synchrotron x-ray source, $|P|$ can be approximated by 1.

Molybdenum emits huge amounts of fluorescence and characteristic x-rays when it receives high energy beam. The x-rays increase the background scattering in the powder diffraction data as shown in figure 1(A). Figure 1(A) shows the powder profile of the 620 Bragg reflection. The ratio of the standard uncertainty to the Bragg intensity exceeds 1.6%. In this study, the combination of copper and nickel foils attached to the front of the IP was used to reduce the x-ray fluorescence from the molybdenum. Figure 1(B) shows the powder profile of the 620 Bragg reflection using metal foils. The ratio of the standard uncertainty to the Bragg intensity improved to 0.92%. The multiple overlaid measurements with the metal foils was effective for improving the precision of

Table 1. Multipole parameters for the experimental and theoretical structure factors.

	30 K	WIEN2k
R_F (%)	0.56	0.20
GOF	0.7879	1.8773
Scale	1.0050(4)	1.5033(4)
κ	0.871(9)	1
κ'	0.9013(9)	0.9741(8)
H0	−0.0035(7)	−0.0021(4)
H4+	−0.0026(6)	−0.0016(3)

the measured structure factors. The ratios of the uncertainties and structure factors of the lowest 16 reflections were better than 0.004.

The Rietveld refinements using multiple datasets were carried out using the program Synchrotron Powder (SP) [29]. The reciprocal resolution in the analysis corresponds to $\sin\theta/\lambda = 2.32$ Å^{-1}. The observed structure factors were initially extracted from the results of the Rietveld refinements based on the independent atom model (IAM). The reliability factors based on the weighted profile R_{wp} and the Bragg intensity R_I of the final pattern fitting were 0.0253 and 0.0133, respectively. The determined lattice constants, a, and the isotropic atomic displacement parameter, u_{iso}, were 3.142 600(1) Å and 0.000 837(3) Å^2, respectively. The estimated isotropic atomic displacement parameter using $u_{iso}^{D} = (3h^2T)/(4\pi^2 m k_B \theta_D)$ [31] is 0.001 04, where h is the Planck constant, T is temperature, m is atomic mass, k_B is the Boltzmann constant, and θ_D is the Debye temperature $\theta_D = 380$ K. $u_{iso}/u_{iso}^{D} = 0.805$ is consistent with the case of aluminum which value is 0.804 using 0.002 893(8) and 0.003 597 of u_{iso} and u_{iso}^{Theo}, respectively.

The intensity ratio of completely overlapped Bragg reflections was determined by the multipole refinement. Table 1 shows the reliability factor and multipole parameters by XD2016 [32] for the experimental structure factors. The electron configuration of molybdenum was $1s^2\,2s^2\,2p^6\,3s^2\,3p^6\,3d^{10}\,4s^2\,4p^6\,4d^5\,5s^1$. We set $4d^5$ valence electron shell. The local axes for the molybdenum atom were parallel to the [100], [010], and [001] directions. The scale factor s, isotropic thermal displacement, u_{iso}, radial expansion/contraction parameters for the spherical valence, κ, aspherical valence, κ', and the hexadecapole parameter, H0, were refined in the analysis. There is a relationship between H0 and H4+, where H4+ = 0.74048H0.

We also prepared theoretical structure factors with the same reciprocal resolution of the observed data using the WIEN2k program [33]. The first principle calculation based on the density functional theory was performed using the full potential-linearized augmented plane wave (FP-LAPW) with the generalized gradient approximation (GGA) in the package. Experimental lattice constants were used for the calculations. We used 1000 k points with a plane-wave cutoff parameter of $R^{MT}K_{max} = 7.0$. The theoretical structure factors were calculated by the lapw3 program. The charge density from the theoretical structure factors was also determined by a multipole modelling. The reliability factor and multipole parameters are also listed in table 1.

3. Results

3.1. Structure factors

The present experimental and theoretical structure factors are listed in table 2. The structure factors of the IAM, f_{IAM} and LCGO, f_{LGCO}, by Jani *et al* [26] are also listed in the table. The values are listed as form factors divided by the phase factor. The sixteen lower resolution values are also shown in the table. We call the present observed structure factors f_{OBS}, and the theoretical structure factors by WIEN2k f_{WIEN}. The first two f_{OBS}, f_{WIEN}, and f_{LCGO} were smaller than or equal to the corresponding f_{IAM}.

Figure 2 shows plots of the relative ratio of the structure factors to f_{IAM} for f_{OBS}, f_{WIEN}, and f_{LCGO}. The deviations from f_{IAM} in the lowest two f_{OBS}, f_{WIEN} and f_{LCGO} are also well recognized in the figure. The structure factors with resolutions better than 0.4 Å^{-1} were almost the same as those of f_{IAM} within experimental uncertainties. The key features that deviated from the IAM were mainly included in the first two reflections. The maximum deviation of the structure factors from the f_{IAM} was less than 2% in the f_{OBS}, f_{WIEN} and f_{LCGO}. The deviations include information on the aspherical distribution of the d-electrons.

3.2. Valence charge density map

Figure 3 shows valence charge density maps for 110 plane from the multipole refinements of the (A) present observed and (B) theoretical (WIEN2k) structure factors. Contour lines were drawn from 0.0 to 2.0 with a step

Table 2. The lowest 16 structure factors of the present study and LCGO. f_{OBS} and f_{WIEN} denote the present experimental and theoretical structure factors. f_{IAM} was calculated by XD2016. f_{LCGO} is the theoretical results [26].

hkl	f_{OBS}	f_{WIEN}	f_{IAM}	f_{LCGO}
110	31.31(4)	31.62	31.84	31.59
200	27.11(5)	27.56	27.56	27.49
211	24.71(4)	25.10	24.91	24.98
220	22.73(5)	23.23	23.07	23.11
310	21.19(4)	21.72	21.68	21.62
222	20.24(6)	20.69	20.58	20.58
321	19.20(4)	19.70	19.66	19.60
400	18.35(8)	18.80	18.86	18.70
330	17.55(6)	18.16	18.15	18.05
411	17.56(5)	18.12	18.15	18.01
420	16.92(5)	17.49	17.50	17.37
332	16.35(5)	16.92	16.90	16.81
422	15.84(5)	16.35	16.35	16.23
431	15.24(4)	15.82	15.83	15.70
510	15.24(5)	15.79	15.83	15.67
521	14.12(4)	14.85	14.87	14.73

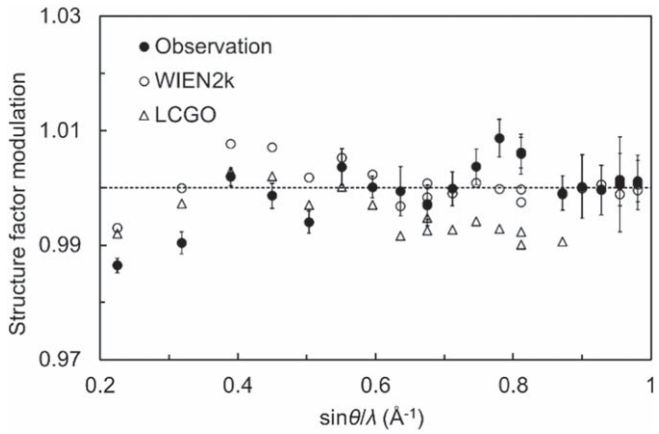

Figure 2. Plots of relative ratio of structure factors to IAM. Horizontal axis represents reciprocal resolution sin θ/λ. Vertical axis represents the relative ratio. Closed circles, open circles, and open triangles are relative ratio for f_{OBS}, f_{WIEN}, and f_{LCGO}, respectively. For f_{OBS}, effect of temperature factor was excluded. Dotted line represents relative ratio of 1.

width of 0.1 e Å^{-3}. The centers and corners of the figures present the atomic sites. The map of the same section was reported by [27]. There are four peaks around the atomic sites in figure 3(A) and (B). These peaks were also found in the previous study [27]. The distances between the peaks and the atomic site for observation and WIEN2k were 0.574 and 0.557 Å, respectively. The charge densities at the maxima for observation and WIEN2k were 1.1 and 1.3 e Å^{-3}, respectively. The features of the present observation are well-consistent with the theory. The numerical differences were 0.017 Å in distance and 0.2 e Å^{-3} in charge density.

3.3. Static deformation density map and d-orbital population

Figure 4 shows static deformation density maps for 110 plane of (A) observation and (B) WIEN2k. Contour lines were drawn from −0.3 to 0.3 with a step width of 0.05 e Å^{-3}. The static deformation density is the difference between the multipole model density and the IAM without effects of thermal smearing. The $d_{3z2\text{-}r2}$ shaped negative regions along the up-down direction were found in both figures. In addition, an excess of the charge density was found in the diagonal directions. We have numerically estimated the electron occupancies of the 4*d*-orbitals of molybdenum. The quantization axes were parallel to the crystal axes as shown in figure 4.

Table 3 lists the *d*-orbital occupancies of molybdenum of observation and WIEN2k. The *d*-electrons of molybdenum can occupy two types of orbitals. One is triply generate Γ'_{25}, dγ and the other is doubly generate Γ_{12}, dε. Γ'_{25} is d_{xy}, d_{yz}, and d_{zx} and Γ_{12} is d_{x2y2} and d_{3z2r2}. Occupancies of the two orbitals are also listed in the table. It was found that almost 0.5 electron decreased from the Γ_{12} orbital in the result of the observation. The

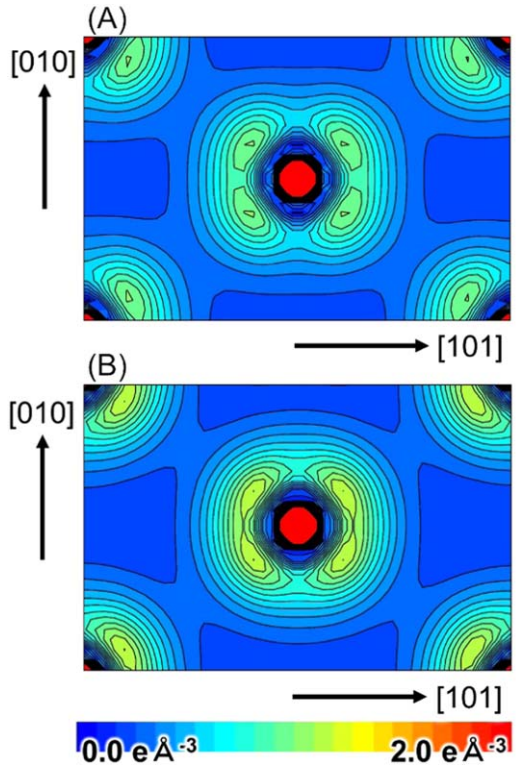

Figure 3. Valence charge density maps of (A) observation and (B) WIEN2k for (110) plane. The contour lines were drawn from 0.0 to 2.0 with 0.1 e $Å^{-3}$ step width. Color bar is also shown at the bottom.

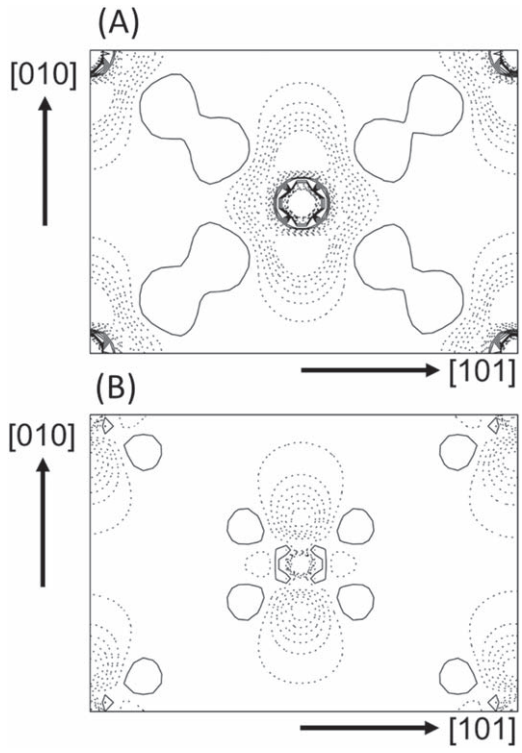

Figure 4. Static deformation density maps of (A) observation and (B) WIEN2k for (110) plane. The contour lines were drawn from −0.30 to 0.30 with 0.05 e $Å^{-3}$ step width. Solid and dashed lines represent positive and negative density, respectively.

Table 3. The *d*-orbital populations for observation and WIEN2k.

Orbital	$^{OBS}d_{pop}$	$^{OBS}d_{occ}$	$^{WIEN}d_{pop}$	$^{WIEN}d_{occ}$
z^2	0.767 19	15.3%	0.861 08	17.2%
xz	1.158 41	23.1%	1.095 82	21.9%
yz	1.158 41	23.1%	1.095 82	21.9%
x^2-y^2	0.766 34	15.3%	0.857 55	17.1%
xy	1.159 09	23.1%	1.099 25	21.9%

Table 4. Charge density ρ and Laplacian $\nabla^2\rho$ at BCP for observation and WIEN2k.

ρ_{OBS}	$\nabla^2\rho_{OBS}$	ρ_{WIEN}	$\nabla^2\rho_{WIEN}$
0.373	3.123	0.326	3.174

numbers of deficient and excess electrons of observation was approximately 0.2 electrons different from those of WIEN2k indicating the more aspherical feature of the valence electron of observation.

The topological properties of the charge density for observation and WIEN2k were calculated. The charge densities and Laplacians at the bond critical point (BCP) are listed in table 4. The charge density and Laplacian of observation were 0.04 e $Å^{-3}$ higher and 0.06 e $Å^{-5}$ lower than those of WIEN2k, respectively. These facts suggest the more covalent bonding character of observation than that of WIEN2k.

4. Conclusion

We completed an experimental charge density study of a 4*d*-transition metal, molybdenum, using state of the art SR-HXRD at SPring-8. Sufficient deviations from the IAM in the structure factors were observed in the first two reflections and the origin of the deviations was revealed by the charge density study by multipole modelling. Solid crystalline molybdenum was formed by the covalent bonding of the Γ'_{25} *d*-orbitals. The bonding contributes to the hardness of the molybdenum solid. The present charge density study supports this picture of solid molybdenum as a hard material. The present study also reveals that molybdenum has more covalent bonding character than the theoretical calculation by WIEN2k with the GGA basis set. We have recently observed a small amount of tight-binding like electron in pure aluminum by SR-HXRD [34]. The chemical bonding was similar to the presently observed covalent bonding character. These studies imply that valence electrons in a pure metal system have a more atomic orbital like character than that expected by the DFT theory.

The less than 0.5 electron deficiency of the orbitals was clearly recognized by the *d*-orbital population analysis and the spatial distribution of the 4*d*-electrons was well recognized in the valence and static deformation density maps in the present study. These facts suggest that the spatial structure of a 4*d*- system can be experimentally revealed by the present SR-HXRD. Novel physical properties are found in 4*d*- and 5*d*-system such as the superconductivity of Sr_2RuO_4 [35] and the metal-insulator transition in $Cd_2Os_2O_7$ [36]. The present experimental and analytical techniques easily apply to these systems by changing the sample and temperature.

The quality of high-energy quantum beam x-ray and electron beam has been drastically improved throughout the past decade such as with x-ray laser, etc. A state of the art high-energy quantum beam enables us to open a new door in subatomic scale studies. The 4*d*- and 5*d*-system with novel physical properties will be a promising target of high-energy quantum beam science.

Acknowledgments

This work was supported by JSPS KAKENHI Grant Numbers JP17J06100(T. S.), JP17H05328 (E. N.), 18H04499 (E. N.) and JP18K14136 (H. K.). This work was also partly supported by CASIO SCIENCE PROMOTION FOUNDATION. The synchrotron experiments were performed at SPring-8 with the approval of the Japan Synchrotron Radiation Research Institute (JASRI) (Proposal No. 2016B1754, 2017A0074, 2017B0074, 2018A0074, 2018B0074 and 2019A0068).

ORCID iDs

Eiji Nishibori https://orcid.org/0000-0002-4192-6577

References

[1] Imada M, Fujimori A and Tokura Y 1998 *Rev. Mod. Phys.* **70** 1039–263
[2] Bednorz J G and Muller K A 1986 *Z. Phys. B Cond. Mat.* **64** 189–93
[3] Maeno Y, Hashimoto H, Yoshida K, Nishizaki S, Fujita T, Bednorz J G and Lichtenberg F 1994 *Nature* **372** 532–4
[4] Jauch W and Reehuis M 2006 *Phys. Rev.* B **73** 085102
[5] Jauch W and Reehuis M 2007 *Phys. Rev.* B **76** 235121
[6] Jauch W and Reehuis M 2008 *Phys. Rev.* B **78** 235113
[7] Jauch W and Reehuis M 2009 *Phys. Rev.* B **80** 125126
[8] Jauch W and Reehuis M 2011 *Phys. Rev.* B **83** 115102
[9] Temkin R J, Henrich V E and Raccah P M 1972 *Phys. Rev.* B **6** 3572–81
[10] Schmokel M S *et al* 2013 *Acta Cryst.* A **69** 570–82
[11] Craven M, Nygaard M H, Zadrozny J M, Long J R and Overgaard J 2018 *Inorg. Chem.* **57** 6913–20
[12] Ehrenreich H and Philipp H R 1962 *Phys. Rev.* **128** 1622–9
[13] Blodgett A J Jr and Spicer E W 1966 *Phys. Rev.* **146** 390–402
[14] Ehrenreich H, Philipp H R and Olechna D J 1963 *Phys. Rev.* **131** 2469–77
[15] Biondi M A and Rayne J A 1959 *Phys. Rev.* **115** 1522–30
[16] Ley L, Pollak R A, McFeely F R, Kowalczyk S P and Shirley D A 1974 *Phys. Rev.* B **9** 600–21
[17] Arima T, Tokura Y and Torrance J B 1993 *Phys. Rev.* B **48** 17006–9
[18] Callcott T A and Mac Rae A U 1969 *Phys. Rev.* **178** 966–78
[19] de Groot F M F, Fuggle J C, Thole B T and Sawatzky G A 1990 *Phys. Rev.* B **42** 5459–68
[20] Jeon Y, Chen J and Croft M 1994 *Phys. Rev.* B **50** 6555–63
[21] Saka T and Kato N 1986 *Acta Cryst.* A **42** 469–78
[22] Nakashima P N H, Smith A E, Etheridge J and Muddle B C 2011 *Science* **331** 1583–6
[23] Kasai H *et al* 2018 *Nat. Mater.* **17** 249–52
[24] Kasai H and Nishibori E 2017 *Sci. Rep.* **7** 41375
[25] Zunger A, Kerker G P and Cohen M L 1979 *Phys. Rev.* B **20** 581–93
[26] Jani A T, Tripathi G S, Brener N E and Callaway J 1989 *Phys. Rev.* B **40** 1593–602
[27] Brandt G B and Rayne J A 1963 *Phys. Rev.* **132** 1945–63
[28] Leaver G and Myers A 1969 *Phil. Mag.* **19** 465–75
[29] Nishibori E, Sunaoshi E, Yoshida A, Aoyagi S, Kato K, Takata M and Sakata M 2007 *Acta Cryst.* A **63** 43–52
[30] Suortti P 1982 *Acta Cryst.* A **38** 642–7
[31] Warren B E 1990 *X-ray Diffraction* (New York: Dover Pub. Inc.)
[32] Volkov A, Macchi P, Farrugia L J, Gatti C, Mallinson P, Richter T and Koritsanszky T 2016 *XD2016 - A Computer Program Package for Multipole Refinement, Topological Analysis of Charge Densities and Evaluation of Intermolecular Energies from Experimental and Theoretical Structure Factors* (Italy: University at Buffalo, State University of New York, University of Milano, University of Glasgow, CNR-ISTM, Middle Tennessee State University)
[33] Blaha P, Schwarz K, Madsen G K H, Kvasnicka D and Luitz J 2001 *WIEN2k, an Augmented Plane Wave plus Local Orbitals Program for Calculating Crystal Properties* (Austria Wien: Technische Universitat)
[34] Sasaki T, Kasai H and Nishibori E 2018 *Sci. Rep.* **8** 11964
[35] Kittaka S, Taniguchi H, Yonezawa S, Yaguchi H and Maeno Y 2010 *Phys. Rev.* B **81** 180510
[36] Yamaura J *et al* 2012 *Phys. Rev. Lett.* **108** 247205